

# Time-reversal simulations for detection in randomly layered media

Mansoor A Haider<sup>1</sup>, Kurang J Mehta<sup>2</sup> and Jean-Pierre Fouque<sup>1</sup>

<sup>1</sup> Department of Mathematics, Box 8205, North Carolina State University, Raleigh, NC 27695-8205, USA

<sup>2</sup> Department of Geophysics, Colorado School of Mines, Golden, CO 80401-1887, USA

Received 5 June 2003, in final form 9 December 2003

Published 17 March 2004

Online at [stacks.iop.org/WRM/14/185](http://stacks.iop.org/WRM/14/185) (DOI: 10.1088/0959-7174/14/2/007)

## Abstract

A time-reversal mirror is, roughly speaking, a device which is capable of receiving an acoustic signal in time, keeping it in memory and sending it back into the medium in the reversed direction of time. In this paper, we employ an accurate numerical method for simulating waves propagating in complex one-dimensional media. We use numerical simulations to reproduce the time-reversal self-averaging effect which takes place in randomly layered media. This is done in the regime where the inhomogeneities are smaller than the pulse, which propagates over long distances compared to its width. We show numerical evidence for possible use of an expanding window time-reversal technique for detecting anomalies buried in the medium.

## 1. Introduction

A time-reversal mirror is, roughly speaking, a device which is capable of receiving an acoustic signal in time, keeping it in memory and sending it back into the medium in the reversed direction of time. In the context of ultrasounds, time-reversal mirrors have been developed and their effect studied experimentally by Mathias Fink and his collaborators at the Laboratoire Ondes et Acoustique (ESPCI-Paris) [8, 9]. The main effect is the refocusing of the scattered signal after time reversal in a random medium: an acoustic pulse is sent in a disordered medium generating a ‘noisy’ reflected signal which is time reversed and sent back into the medium. The new reflected signal is a pure pulse with a shape similar to the initial pulse. Amazingly, its ‘refocusing’ takes place in time and space and seems to be independent of the realization of the medium, in the regime where its correlation length is smaller than the typical wavelength of the pulse.

From the theoretical point of view, a first proof of this refocusing effect has been obtained in [7] in the context of a one-dimensional random medium for which only the time refocusing

is relevant. The refocusing is obtained by using asymptotics in the regime where there are three well-separated scales:

$$\frac{\text{correlation length of the medium}}{\text{wavelength of the pulse}} \approx \frac{\text{wavelength of the pulse}}{\text{distance of propagation}} \ll 1.$$

The fluctuations of the medium are not assumed to be small but rather of the order of several tens of per cent. In the case of a stationary random medium, a theoretical formula for the limiting refocused pulse is given in [7]. It shows that the refocused pulse is a convolution of the initial pulse with a kernel that depends on the cut-off of the reflected signal and on the autocorrelation of the medium. In the non-stationary case, which is the case for the detection problem considered in this paper, there is no explicit formula available.

In this study, we write a numerical method in the frequency domain for the one-dimensional (1D) wave equation and use it to study the time-reversal refocusing effect for waves propagating through a scatterer comprising many layers with randomly varying wave speed. On each layer of the scatterer, our method yields two relations in terms of the unknown field and its normal derivative on the interfaces of that layer. When matched to an incident field on the first interface, our approach is analogous to a transfer matrix method [1] that is formulated in the frequency domain. We derive our 1D method via a boundary integral equation approach in the frequency domain to facilitate future extension to higher dimensions. For example, in 2D, a boundary integral method has been developed and used to study resonant modes for electromagnetic scattering in photonic crystal slabs [11]. A frequency domain boundary integral formulation is also the appropriate context for implementation of a fast multipole method [13]. Using our 1D method, we simulate the time-reversal refocusing effect in reflection, and analyse the potential for using time reversal in detecting the presence of an extended strong scatterer buried in the random medium. The inverse problem, which consists of reconstructing the large scale variations of the medium (its slowly varying component), is an extremely challenging problem. It has been addressed in [1, 2] and [12] by using reflected signals. Theoretically, the slowly varying components of the medium parameters appear in the coefficients of an infinite system of transport equations [1] and this makes the inverse problem very delicate. In this paper, we propose to tackle numerically a simpler problem (i.e. detection of an anomaly of size larger than the typical inhomogeneities), by using an expanding window time-reversal technique (section 4.2) and, in particular, by exploiting the self-averaging property of the refocused pulses.

Time reversal in several dimensions has been studied in various regimes: for instance, in [5] in the parabolic approximation regime, in [10] in the case of a point source in a randomly layered medium and in [3] for general waves propagating in weakly fluctuating media. Recent applications to imaging can be found in [6]. The numerical method presented here in the context of strongly contrasted media is well adapted to multi-dimensional generalizations which are part of our future work.

## 2. Formulation of interface equations in the frequency domain

Our numerical formulation is based on a frequency domain boundary integral method which, in the 1D context, yields a transfer matrix for the unknown components of the field and its normal derivative on each layer interface. While in 1D, our method is not particularly novel, the frequency domain boundary integral formulation can be extended to simulate time reversal in higher dimensions, where theory is available only in special cases. Extension of the numerical method is briefly discussed in section 2.5.

### 2.1. Green's functions in the frequency domain

We consider the one-dimensional wave equation for a field  $u(x, t)$ :

$$\frac{\partial^2 u}{\partial t^2} = c^2(x) \frac{\partial^2 u}{\partial x^2}, \quad x \in \Omega, \quad t > 0 \quad (1)$$

where  $\Omega = (-\infty, \infty)$  and  $c(x)$  is the wave speed. Let  $\Omega = (-\infty, a_0) \cup \Omega_0 \cup \dots \cup \Omega_{N-1} \cup (a_N, \infty)$  where  $\Omega_j = (a_j, a_{j+1})$ ,  $j = 0, \dots, N-1$  ( $a_0 < a_1 < \dots < a_N$ ). A layered medium is considered by taking  $c(x)$  to be piecewise constant on  $\Omega$  as follows:

$$c(x) = \begin{cases} c_j & \text{for } x \in \Omega_j, j = 0, 1, \dots, N-1 \\ c' & \text{for } x \in (-\infty, a_0) \cup (a_N, \infty). \end{cases} \quad (2)$$

We consider the case in which the continuous quantities on the interfaces  $x = a_0, \dots, a_N$  are  $u$  and  $\frac{\partial u}{\partial x}$ . Denote by  $\hat{F}(\omega)$  the Fourier transform in time of a function  $f(t)$  ( $\hat{F}(\omega) = \int_{-\infty}^{\infty} f(t) e^{i\omega t} dt$ ).

Taking the Fourier transform of (1) using (2), we obtain the following Helmholtz equations for each frequency  $\omega$  ( $-\infty < \omega < \infty$ ):

$$\frac{\partial^2 \hat{u}}{\partial x^2} + k_j^2 \hat{u} = 0, \quad x \in \Omega_j \quad (k_j = \omega/c_j) \quad (3)$$

$$\frac{\partial^2 \hat{u}}{\partial x^2} + k^2 \hat{u} = 0, \quad x \in (-\infty, a_0) \cup (a_N, \infty) \quad (k = \omega/c'). \quad (4)$$

Introduce a Green's function  $\hat{H}^j(x, y) = (2ik_j)^{-1} e^{ik_j|x-y|}$  for each layer  $\Omega_j$  of the medium, and a free space Green's function  $\hat{H}(x, y) = (2ik)^{-1} e^{ik|x-y|}$ . These Green's functions give rise to outward radiating waves at  $x = -\infty$  and satisfy equations (3) and (4), respectively, with a non-homogeneous singular source term  $\delta(x-y)$ , where  $\delta(x)$  is the Dirac delta function.

### 2.2. Interior representations

To represent the field  $\hat{u}$  in the interior of layer  $\Omega_j$ , we apply reciprocity to (3), integrating on the interval  $\Omega_j = (a_j, a_{j+1})$  to obtain, for  $y \in (a_j, a_{j+1})$ ,

$$\int_{a_j}^{a_{j+1}} \hat{u}(x) \delta(x-y) dx = \int_{a_j}^{a_{j+1}} \left( \frac{\partial^2 \hat{H}^j(x, y)}{\partial x^2} \hat{u}(x) - \hat{H}^j(x, y) \frac{\partial^2 \hat{u}(x)}{\partial x^2} \right) dx. \quad (5)$$

Using the filtering property of  $\delta(x)$  and integration by parts, the domain integrals cancel out and (5) reduces to

$$\begin{aligned} \hat{u}(y) = & \frac{\partial \hat{H}^j(a_{j+1}, y)}{\partial x} \hat{u}(a_{j+1}) - \frac{\partial \hat{H}^j(a_j, y)}{\partial x} \hat{u}(a_j) - \hat{H}^j(a_{j+1}, y) \frac{\partial \hat{u}(a_{j+1})}{\partial y} \\ & + \hat{H}^j(a_j, y) \frac{\partial \hat{u}(a_j)}{\partial y}, \quad y \in (a_j, a_{j+1}). \end{aligned} \quad (6)$$

Equation (6) determines the field  $\hat{u}$  in the interior of layer  $\Omega_j$  given the (as yet unknown) values of the field  $\hat{u}$  and its normal derivative  $\frac{\partial \hat{u}}{\partial y}$  at the boundaries of the layer.

To obtain an interior representation to the left of the scatterer, consider (6) on the interval  $(a_j, a_{j+1}) = (-L, a_0)$  using the Green's function  $\hat{H}(x, y)$ . As our incident wave, we choose a plane wave propagating from left to right. Hence, the field to the left of the scatterer can be written as  $\hat{u} = e^{iky} + \hat{u}_{sc}$ , where  $\hat{u}_{sc}$  is the scattered wave on  $(-L, a_0)$ . Substituting  $\hat{u}$  into (6), and using the relations  $\hat{H}(-L, y) = (2ik)^{-1} e^{ik(y+L)}$  and  $\frac{\partial \hat{H}(-L, y)}{\partial x} = -\frac{1}{2} e^{ik(y+L)}$ , the second and fourth terms of (6) reduce to  $e^{iky}$ . Taking the limit as  $L \rightarrow \infty$ , an interior representation for

the reflected field to the left of the scatterer is obtained:

$$\hat{u}(y) = \frac{\partial \hat{H}(a_0, y)}{\partial x} \hat{u}(a_0) - \hat{H}(a_0, y) \frac{\partial \hat{u}(a_0)}{\partial y} + e^{iky}, \quad y \in (-L, a_0). \quad (7)$$

Similarly, by considering (6) on the interval  $(a_N, L)$ , where there is no incident wave, the limit as  $L \rightarrow \infty$  yields the following interior representation for the transmitted field to the right of the scatterer:

$$\hat{u}(y) = -\frac{\partial \hat{H}(a_N, y)}{\partial x} \hat{u}(a_N) + \hat{H}(a_N, y) \frac{\partial \hat{u}(a_N)}{\partial y}, \quad y \in (a_N, \infty). \quad (8)$$

### 2.3. Formulation of a system of equations in the interface unknowns

It remains to determine the unknown values of the field  $\hat{u}$  and its normal derivative  $\frac{\partial \hat{u}}{\partial y}$  on the interfaces  $y = a_0, a_1, \dots, a_N$ . Using a boundary integral method, we obtain a closed system of linear algebraic equations for these unknowns by taking the limit as the interior point  $y$  approaches the two boundary points of each layer.

Consider the interior representation (6) in layer  $\Omega_j$  of the medium. Taking the limit as  $y \rightarrow a_j^+$ , and using the fact that  $\frac{\partial \hat{H}^j(a_j, a_j^+)}{\partial x} = -1/2$  and  $\hat{H}^j(a_j, a_j^+) = (2ik_j)^{-1}$ , we obtain a relation in terms of the interface unknowns for layer  $\Omega_j$  ( $j = 0, 1, \dots, N-1$ ):

$$\frac{1}{2} \hat{u}(a_j) - \frac{1}{2ik_j} \frac{\partial \hat{u}(a_j)}{\partial y} = \frac{\partial \hat{H}^j(a_{j+1}, a_j^+)}{\partial x} \hat{u}(a_{j+1}) - \hat{H}^j(a_{j+1}, a_j^+) \frac{\partial \hat{u}(a_{j+1})}{\partial y}. \quad (9)$$

Similarly, taking the limit of (6) as  $y \rightarrow a_{j+1}^-$  and using the fact that  $\frac{\partial \hat{H}^j(a_{j+1}, a_{j+1}^-)}{\partial x} = 1/2$  and  $\hat{H}^j(a_{j+1}, a_{j+1}^-) = (2ik_j)^{-1}$ , we obtain a second relation involving the interface unknowns for layer  $\Omega_j$  ( $j = 0, 1, \dots, N-1$ ):

$$\frac{1}{2} \hat{u}(a_{j+1}) + \frac{1}{2ik_j} \frac{\partial \hat{u}(a_{j+1})}{\partial y} = -\frac{\partial \hat{H}^j(a_j, a_{j+1}^-)}{\partial x} \hat{u}(a_j) + \hat{H}^j(a_j, a_{j+1}^-) \frac{\partial \hat{u}(a_j)}{\partial y}. \quad (10)$$

Equations (9) and (10) comprise  $2N$  equations in the  $2N+2$  interface unknowns. The remaining two equations are obtained by performing a similar limiting process on intervals to the left and right of the layered medium to obtain, respectively:

$$\frac{1}{2} \hat{u}(a_0) + \frac{1}{2ik} \frac{\partial \hat{u}(a_0)}{\partial y} = e^{ika_0} \quad \text{and} \quad \frac{1}{2} \hat{u}(a_N) - \frac{1}{2ik} \frac{\partial \hat{u}(a_N)}{\partial y} = 0. \quad (11)$$

The closed system of equations for the  $2N+2$  unknown values of the  $\hat{u}$  and  $\frac{\partial \hat{u}}{\partial y}$  on the interfaces located at  $y = a_0, \dots, x = a_N$  consists of (9), (10) (for  $j = 0, 1, \dots, N-1$ ) and (11). This system of equations is assembled into a banded matrix (bandwidth 5) that is effectively a transfer matrix for the unknown components of the field and its normal derivative on the layer interfaces. Solutions of the linear system are obtained at each frequency  $\omega$  using a banded solver which, for  $N$  layers, requires  $O(N)$  operations.

### 2.4. Example: calculating reflection and transmission amplitudes

Once the interface unknowns are determined via solution of (9)–(11) at a particular reduced frequency  $k = \omega/c'$ , the transmitted wave on the interval  $y \in (a_N, \infty)$  is determined from (8) as

$$\hat{u}_{\text{tr}}(y) = \hat{T}(k) e^{iky}, \quad \text{where} \quad \hat{T}(k) = \frac{e^{-ika_N}}{2} \left( \hat{u}(a_N) + \frac{1}{ik} \frac{\partial \hat{u}(a_N)}{\partial y} \right). \quad (12)$$

Similarly, the reflected wave on the interval  $y \in (-\infty, a_0)$  is determined from (7) as

$$\hat{u}_{\text{ref}}(y) = \hat{R}(k) e^{-iky} + e^{iky}, \quad \text{where} \quad \hat{R}(k) = \frac{e^{ika_0}}{2} \left( \hat{u}(a_0) - \frac{1}{ik} \frac{\partial \hat{u}(a_0)}{\partial y} \right). \quad (13)$$

### 2.5. Extension of the boundary integral method to higher dimensions

While in 1D, equations (9)–(11) yield a banded transfer matrix, their formulation using a boundary integral approach extends to the development of numerical methods for multiple scattering in higher dimensions. For example, in higher dimensions the layers  $\Omega_j$  can be closed regions that define scatterers, with prescribed geometric and material properties, that are embedded in a homogeneous background medium. In the interior representation (6), the right-hand side becomes a line integral (2D) or surface integral (3D) written in terms of the field and its normal derivative on the scatterer interfaces. The 1D Green's functions for the Helmholtz equation are replaced by higher dimensional counterparts interior and exterior to the scatterers. The limiting process of section 2.3 yields a closed system of boundary integral equations on either a collection of closed contours (2D) or closed surfaces (3D). These integral equations are solved numerically using a collocation method to obtain approximations to the field and its normal derivative on the scatterer interfaces. Equation (12) for the transmitted field and equation (13) for the reflected field then involve integrals written in terms of the computed field approximations over the union of scatterer interfaces. In higher dimensions, boundary integral methods reduce the computational mesh by one dimension at the expense of a fully populated linear system in the collocation. However, analytical manipulation of the Green's functions can be used to uncouple near and far-field effects, leading to sparse linear systems and significant acceleration of the numerical solution of the governing boundary integral equations.

Using the approach described above, 2D boundary integral numerical methods were developed for analysis of bandgaps and resonances in 2D photonic crystal slabs (finite in  $X$ , periodic in  $Y$ , homogeneous in  $Z$ ) [4, 11, 14]. These methods were used to conduct a parametric analysis of resonance quality for Fabry–Perot laser cavities comprising circular dielectric rods in both the lossless [14] and lossy [4] cases. Via analytical manipulation of the 2D Green's function, the formulation was accelerated in [11] to give a method that was  $O(\tilde{N})$  in the direction of finite extent ( $X$ ), where  $\tilde{N}$  is the number of interface collocation points. This fast method was used to compute complete photonic bandgaps (i.e. for all incident angles) with random perturbations in crystal geometry, and to analyse resonance quality in the presence of channel defects. Formulations for the development of efficient boundary integral numerical methods in the general 2D and 3D cases are presented by Rokhlin in [13]. These studies can serve as the basis for numerical simulation of time reversal in higher dimensions, where theoretical results are available only in special cases. However, efficient and accurate analysis in higher dimensions poses a challenging computational problem due to the inherent random and multi-scale nature of the time-reversal effect.

## 3. Time reversal in the frequency domain

We now formulate time reversal of a reflected pulse in terms of the reflection scattering operator  $\hat{R}(k)$  given in (13). Consider a unit-amplitude Gaussian derivative pulse  $u_{\text{inc}}(y, t) = f\left(\frac{y-y_0-c't}{\epsilon}\right)$  that is centred at  $y = y_0$  when  $t = 0$ , where  $f(x) = -\sqrt{\epsilon} x \epsilon e^{-x^2/2}$  and  $\epsilon$  is a characteristic wavelength of the pulse. With this normalization the maximum value of  $|f|$  is exactly 1. The Fourier transform of the pulse is

$$\hat{u}_{\text{inc}}(y, \omega) = \frac{1}{c'} e^{i\omega(y-y_0)/c'} i\omega\sqrt{2\pi}\epsilon e^2 e^{-\epsilon^2\omega^2/(2c'^2)} \quad (14)$$

$$= \hat{A}(\omega/c') e^{i\omega y/c'}, \quad \text{where} \quad \hat{A}(k) = \sqrt{2\pi}\epsilon e^2 ik e^{-ik y_0} e^{-\epsilon^2 k^2/2}. \quad (15)$$

By (13), the reflected signal to the left of the scatterer is given by

$$\hat{u}_{\text{ref}}(y, \omega) = \hat{A}(\omega/c')(\hat{R}(\omega/c') e^{-i\omega y/c'} + e^{i\omega y/c'}). \quad (16)$$

We now sample a portion of the reflected signal using a window function  $G_{t_0}(t) = H(t) - H(t - t_0)$ , where  $H(t)$  is the Heaviside step function. The window function is used to record a sample of the reflected wave at  $y = y^*$  starting at time  $t = t^*$ . Hence, the reflected wave is sampled for a duration  $t_0$  in the time interval  $t \in (t^*, t^* + t_0)$ . The sample of the reflected signal in the time-domain  $\tilde{u}_{\text{ref}}(t)$  is given by

$$\tilde{u}_{\text{ref}}(t) = u_{\text{ref}}(y, t) G_{t_0}(t - t^* + (y - y^*)/c') \quad (17)$$

where the Fourier transform of  $u_{\text{ref}}(y, t)$  is given by (16). The sampled signal (17) is then reversed in time to obtain a new incident wave  $u_{\text{tr}}(t) = \tilde{u}_{\text{ref}}(t^* + t_0 - t)$ . Using (17), the new incident wave  $u_{\text{tr}}(y, t)$  can be written in the frequency domain as the convolution:

$$\hat{u}_{\text{tr}}(y, \omega) = \frac{1}{2\pi c'} [e^{i\omega(t_0+(y-y^*)/c')} \hat{G}_{t_0}(-\omega)] * [e^{i\omega(t^*+t_0+y_0/c')} (-i\omega)\sqrt{2\pi}\epsilon e^2 e^{-\epsilon^2\omega^2/(2c'^2)} (e^{i\omega y/c'} \bar{\hat{R}}(\omega/c') + e^{-i\omega y/c'})] \quad (18)$$

where  $\bar{\hat{R}}(\omega/c')$  is the complex conjugate of  $\hat{R}(\omega/c')$ . By (13), the second reflection of the new (time-reversed) incident wave is then obtained as  $\hat{u}_{\text{tr}}^{\text{ref}}(y, \omega) = \hat{u}_{\text{tr}}(y, \omega)(\hat{R}(\omega/c') e^{-i\omega y/c'} + e^{i\omega y/c'})$ , which can be written explicitly as

$$\hat{u}_{\text{tr}}^{\text{ref}}(y, \omega) = \frac{i\epsilon^2}{c'} \sqrt{\frac{e}{2\pi}} (\hat{R}(\omega/c') e^{-i\omega y/c'} + e^{i\omega y/c'}) e^{i\omega(t_0+(y-y^*)/c')} \int_{-\infty}^{\infty} \tilde{\omega} \times e^{-\epsilon^2\tilde{\omega}^2/(2c'^2)} e^{i\tilde{\omega}(t^*+(y_0+y^*-y)/c')} (e^{i\tilde{\omega} y/c'} \bar{\hat{R}}(\tilde{\omega}/c') + e^{-i\tilde{\omega} y/c'}) \frac{e^{i(\tilde{\omega}-\omega)t_0} - 1}{i(\tilde{\omega} - \omega)} d\tilde{\omega}. \quad (19)$$

Fourier inversion of (19) gives the time-reversed pulse  $u_{\text{tr}}^{\text{ref}}(y, t)$  in the time domain.

#### 4. Numerical simulations

We employed the method described in section 2.3 in the numerical simulation of time reversal for the wave equation (1) and (2) with wave speeds  $c_j$  in the layers varying randomly about a background velocity  $c' = 1$ . The layered random medium was located on the interval  $[0, 1]$  and layers of a fixed width  $1/N$  were considered by placing the interfaces at  $a_j = j/N$  ( $j = 0, 1, \dots, N$ ). The initial pulse location  $y_0$ , signal recording location  $y$  and time-reversal recording location  $y^*$  were all taken to be one unit to the left of the layered medium (i.e.  $y_0 = y = y^* = -1$ ). Since  $c = c' = 1$  on the left of the layered medium, the time at which sampling of the reflected signal commences was taken as  $t^* = 2$ . The remaining parameters, which control the multiple scales in the problem, are the characteristic pulse wavelength  $\epsilon$ , the number of layers  $N$  and the length of the sampling interval  $t_0$ . This set-up, used in the detection problem in section 4.2, corresponds to an *expanding time window* with  $t^*$  fixed and  $t_0$  increasing. Alternatively, one can consider a *sliding time window* which would correspond to  $t^*$  increasing and  $t_0$  fixed.

For a particular random realization of the layered medium we first computed, at each frequency, the reflection amplitude by solving the linear system (9)–(11) and using the result in (13). We considered a finite number of equally spaced frequencies and, by symmetry, it was sufficient to evaluate all functions in the frequency domain at only non-negative frequencies.

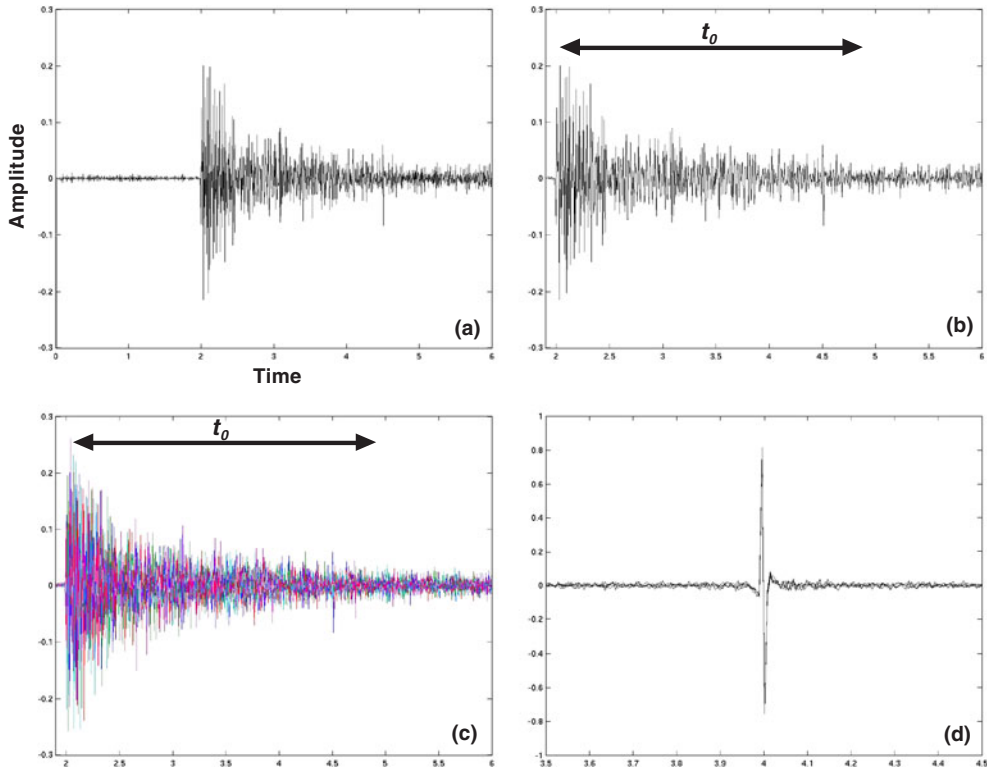


**Figure 1.** A pulse scattered by a randomly layered medium generates a noisy reflected signal shown in (a), and magnified in (b). A simulation with five random realizations (c) shows that the reflected signal depends on the realization of the medium. The reflected signal is sampled using a window of size  $t_0$ , time reversed and sent back into the same medium. Time-reversal refocusing is demonstrated in (d) for five realizations, as well as the self-averaging property of the refocused pulse.

All computations were performed using a 1 GHz dual-processor Apple G4 Power Macintosh in MATLAB 6.5 which employs 16-digit precision. All simulations were conducted for  $N = 1000$  layers and a banded solver was used for rapid and accurate inversion of the coefficient matrix in the assembled linear system. The time-reversed pulse was calculated in the time domain via numerical integration of the convolution integral in (19) followed by a second numerical integration for Fourier inversion. In both cases, Simpson's rule was employed. The same set of sampling frequencies were used in computation of the scattering operator, and in the numerical integration of (19) and the Fourier inversion formula. Once the scales for the layers and pulse were set via  $N$  and  $\epsilon$ , respectively, the frequency resolution required for numerical convergence could be determined. In the finest scale regime considered in this study (i.e.  $N = 1000$ ,  $\epsilon = 0.1/\sqrt{N}$ ), we found that the frequency sampling  $\omega \in (-1000, 1000)$ ,  $\Delta\omega = 0.25$  was sufficient for visual overlapping of successively refined computations of the time-reversed pulse in the time domain.

#### 4.1. Pulse refocusing and self-averaging via time reversal

Numerical simulation of time reversal in reflection is illustrated in figure 1 for the case  $N = 1000$  with  $\epsilon = \frac{1}{r\sqrt{N}}$ ,  $r = 10$  and  $c_j = 1/\sqrt{1 + \eta_j}$ , where  $\eta_j$  is a sequence of i.i.d.

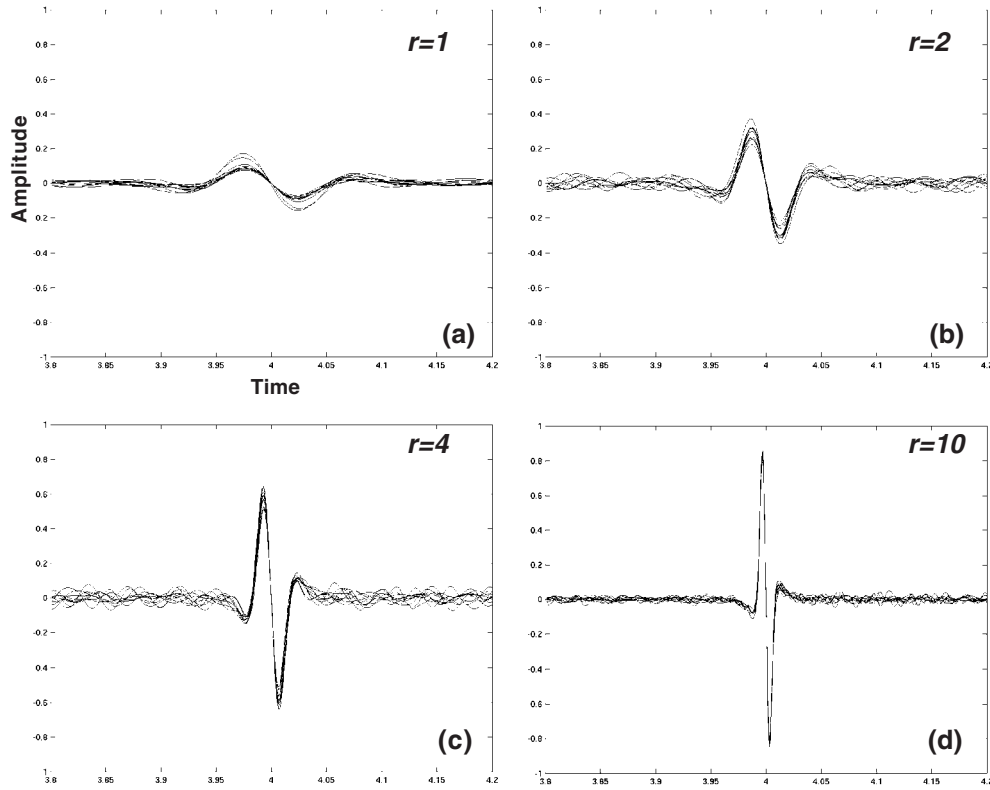


**Figure 2.** Refocusing and self-averaging of the time-reversed pulse is demonstrated as the characteristic pulse wavelength  $\epsilon = \frac{1}{r\sqrt{N}}$  is varied via the parameter  $r$  in the case  $N = 1000$ . The factor  $r$  compensates for a small autocorrelation produced by our i.i.d. medium. It is fixed in the regime where the multiple scales become well separated, and from our experiments (a)–(d) the value  $r = 10$  shows a good tuning of the pulse to the medium in terms of quality of self-averaging of the refocused pulse. For each value of  $r$ , the refocused pulse is shown for ten random realizations of the layered medium.

random variables that are uniformly distributed over the interval  $(-0.8, 0.8)$ . Observe that in the homogenization regime the quantity to be homogenized is  $1/c^2(x)$ , so that the way we modelled the velocity random fluctuations corresponds to centred fluctuations around the homogenized quantity  $\overline{1/c_j^2} = 1$ . The time required to compute the refocused pulse in the time domain for a single realization of the layered medium was roughly 14 min.

At the recording location  $y = -1$ , a typical time signal demonstrating reflection of the incident pulse is shown in figure 1(a). Using the window function  $G_{t_0}$ , a sample of the reflected signal of duration  $t_0$  is recorded (figure 1(b)), reversed in time and then re-introduced into the layered medium as a new incident wave. Multiple realizations demonstrate that the reflected wave does not exhibit a self-averaging property that can capture characteristics of the layered medium (figure 1(c)). In contrast, the reflection of the new (time-reversed) incident wave refocuses the pulse in a manner that is self-averaging with respect to random realizations of wave speed in the component layers of the scattering medium (figure 1(d)).

In figure 2, we illustrate self-averaging and refocusing of the time-reversed pulse as its characteristic wavelength  $\epsilon = \frac{1}{r\sqrt{N}}$  is tuned to the fine scale of the random medium via the parameter  $r$ . For each  $r$ , we computed the time-reversed pulse for ten random realizations of the layered medium. As the pulse wavelength is decreased, separation between the fine

scale of random variation, the intermediate scale of pulse wavelength and the distance of propagation leads to exhibition of the self-averaging property of the refocused pulse when  $r = 10$  (figure 2(d)). In this regime, with  $t_0$  relatively large so that the recording window contains most of the reflected signal, the physical wavelength of the refocused pulse matches that of the original incident pulse with roughly a 12% loss in pulse amplitude due to transmission of waves through the layered medium not yet reflected. Our finding is in agreement with the theoretical formula obtained in [7] which shows that, asymptotically in the regime of separation of scales ( $\epsilon \downarrow 0$ ), the refocused pulse  $f_{\text{tr}}$  is obtained as a convolution  $f_{\text{tr}}(t) = (f(\cdot) \star K(\cdot))(t)$  of the time-reversed initial pulse  $f$  with a kernel  $K$  given by its Fourier transform  $\hat{K}(\omega) = \int_{t^*}^{t^*+t_0} \Lambda(\omega, \tau) d\tau$ . The density  $\Lambda$  is known explicitly in the case of homogenous media. We hypothesize that this self-averaging property of the time-reversed refocused pulse can be employed in detecting the presence of a strong homogeneous scatterer that is buried in the layered random medium. The idea is that  $t_0/2$  corresponds to a depth of penetration and therefore a comparison of the kernels  $\hat{K}$  with and without a buried object produces a detection tool. We choose here not to rely on formulae or computation of the densities  $\Lambda$ , since these will not be available in the multi-dimensional context. Rather, we use a comparison between maxima (amplitudes) of the refocused pulses with and without the buried object.

For practical applications, we suggest that the experiment be repeated at various locations in order to acquire maxima of the refocused pulse without the buried object as a function of  $t_0$ , and then test other locations by comparison as described above. Strictly speaking this is not compatible with the assumed layered structure but one can consider that for remote locations the random layering is independent.

#### 4.2. Detection of a buried extended strong scatterer via time reversal

Numerical simulations were conducted in the self-averaging regime described in the previous section. We hypothesized that time-reversal detection can be evaluated by comparing the distribution of refocused pulse amplitudes over multiple random realizations of the layered medium in the presence and absence of a buried strong scatterer. The strong scatterer is introduced by setting the wave speed for  $L$  layers at a location  $y = y_c$  to  $50c'$ , where  $c'$  is the wave speed in the homogeneous background medium. The case  $L = 100$ ,  $y_c = 0.67$  is illustrated in figure 3(a). A sample realization of the reflected signal for the time-reversal parameters  $t^* = 2.0$ ,  $t_0 = 3.0$  is shown in figure 3(b). We observe that the reflected signal contains no clear signature indicating the presence of a strong scatterer buried in the layered random medium.

*4.2.1. Detecting the presence of the scatterer.* We analysed the effect of the strong scatterer on the amplitude of the time-reversed refocused pulse for multiple time-reversal recording times  $t_0$  (figure 3(c)). An expanding window time-reversal analysis was conducted by increasing the parameter  $t_0$  in increments of 0.5 s up to a value of 3.0 s. For each recording time, we considered ten random realizations with and without a buried strong scatterer. All 100 random realizations in figure 3(c) were independent. As the recording time  $t_0$  is increased to incorporate portions of the reflected signal that correspond to the depth of the buried object (i.e.  $t_0 = 1.5$  s), we observe a statistically significant difference in mean pulse amplitude between the cases with and without a buried strong scatterer. The direct *coherent reflection* from the strong scatterer interface (where  $c$  increases abruptly from 1 to 50) is responsible for this enhancement of the amplitude of the refocused signal. However, due to the strong

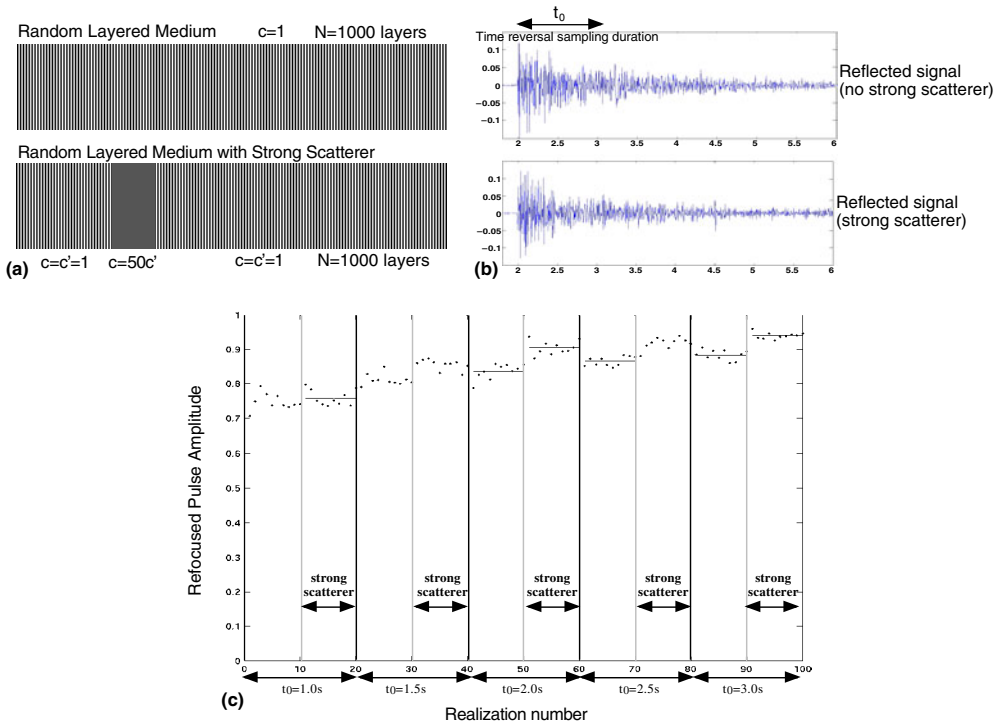


**Figure 3.** Numerical simulations for detection using an expanding window time-reversal analysis ( $N = 1000$  layers,  $\epsilon = \frac{1}{10\sqrt{N}}$ ). (a) Independent realizations of the medium with and without a buried strong scatterer. A pulse is incoming from the right and the scatterer consists of  $L = 100$  layers at a depth  $y_c = 0.67$  with wave speed  $50c'$ . (b) Reflected signals: the coherent reflection due to the strong scatterer is hidden in the noise due to the inhomogeneities. (c) Amplitudes of refocused pulses as the time-reversal window expands (5 windows, 20 independent realizations per window: 10 without buried object and 10 with buried object). Horizontal lines indicate mean amplitudes for each subset of ten realizations.

fluctuations in the medium, this coherent reflection was hidden in the reflected signal, and, in that sense, time reversal reveals it.

Self-averaging of the pulse amplitude improves as the signal recording time is increased to  $t_0 = 3.0$  s. In this self-averaging regime, these results indicate the potential use of the time-reversed refocused pulse as a measure for detection of a buried strong scatterer.

To assess the accuracy of the proposed detection measure, we computed the distribution (i.e. mean, standard deviation) of the refocused pulse amplitude in the case  $t_0 = 3.0$  s for 50 random realizations with and without the presence of the strong scatterer described above. The effect of scatterer size was quantified by varying the parameter  $L$  and the random number generator was assigned a new seed for each value of  $L$ . The computed probability distribution functions are shown in figure 4.

For the case of no scatterer ( $L = 0$ ), the mean pulse amplitude was 0.8786 with a standard deviation of 0.0132 while for the largest buried object considered ( $L = 100$ ) the mean pulse amplitude was 0.9396 with a standard deviation of 0.0151.

For instance, by choosing a detection amplitude threshold at the level 0.91, we find that:

- the probability of error by *false alarm*, that is the area to the right of 0.91 under the  $L = 0$  probability density, is less than 1%;

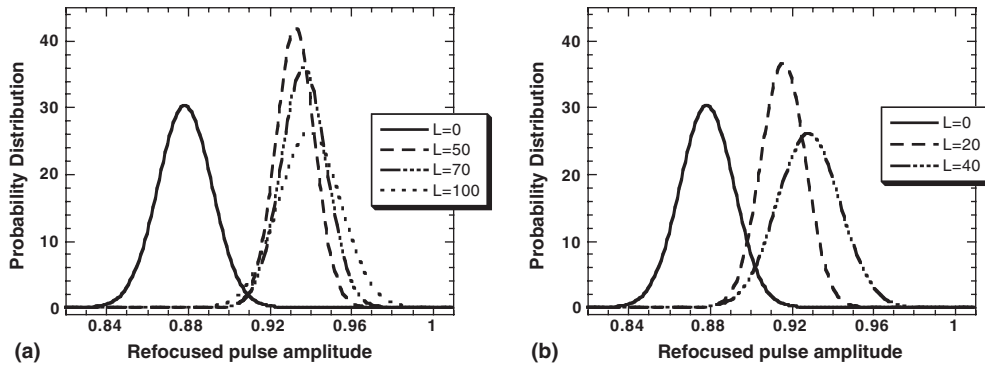


**Figure 4.** Probability distributions of refocused pulse amplitude with varying object size  $L$ . For each buried strong scatterer of size  $L$ , the refocused pulse amplitude was computed for 50 independent random realizations of the layered medium. The mean and standard deviation of the amplitudes were fit to a normal distribution. (a) When the buried strong scatterer is as small as 5% of the size of the layered medium ( $L = 50$ ), the probability of error in the time-reversal detection measure is small. (b) When the size of the buried strong scatterer is below 5% of the size of the layered medium, the probability of error in the time-reversal detection measure increases significantly.

- the *detection power*, that is the probability that the amplitude is greater than 0.91 when the target is present, is over 99% for values of  $L$  as low as  $L = 50$  corresponding to a strong scatterer occupying 5% of the medium;
- the detection power decreases for smaller targets to 88% for  $L = 40$ , and 70% for  $L = 20$ .

**4.2.2. Detecting the location of the scatterer.** The potential use of the refocused pulse amplitude to determine the location of the buried strong scatterer  $y_c$  was analysed in the case  $L = 100$ . We simulated a time-reversal expanding window experiment based on increasing  $t_0$  by increments of 0.2 s in the range 1–3 s and recording the statistics of the refocused pulse amplitude for ten realizations of the reference medium (i.e.  $L = 0$ ). A relatively small number of realizations were used to model potential limitations associated with data collection in practical applications. The expanding window experiment was then repeated for ten independent realizations of the medium with the buried strong scatterer located at  $y = y_c$ . Refocused pulse amplitudes were recorded with increasing  $t_0$  in the cases  $y_c = 0.5, 0.6, 0.7$  (figure 5). In all three cases, it is observed that the refocused pulse amplitude exhibits a statistically significant jump above the distribution of reference pulse amplitudes at a critical value of  $t_0$  that increases with  $y_c$ .

Formulation of a strategy for detecting the location of the buried scatterer was then conducted via analysis of the expanding window data for each realization of the medium. For each realization of expanding window amplitude data, a critical expanding window time  $t_0^*$  was determined using the criterion:

$$t_0^* = \min\{t_0 \in [1, 3] | A(t_1)_{L=100} > \overline{A(t_1)_{L=0}} + 2\sigma\{A(t_1)_{L=0}\}, \quad \forall t_1 \in [t_0, 3]\} \quad (20)$$

where  $A$  is the refocused pulse amplitude and  $\sigma$  is the standard deviation. For each realization, this criterion determines the smallest recording time at which the refocused pulse amplitude exceeds the reference amplitude by  $2\sigma$  in further expansion of the recording window. Note that for larger window size most of the signal would be recorded and consequently the amplitude of the refocused pulse would be the same with or without the buried object. Distributions of  $t_0^*$  with respect to  $t_0$  (over ten realizations) for  $y_c = 0.5, 0.6, 0.7$  are shown using histograms in

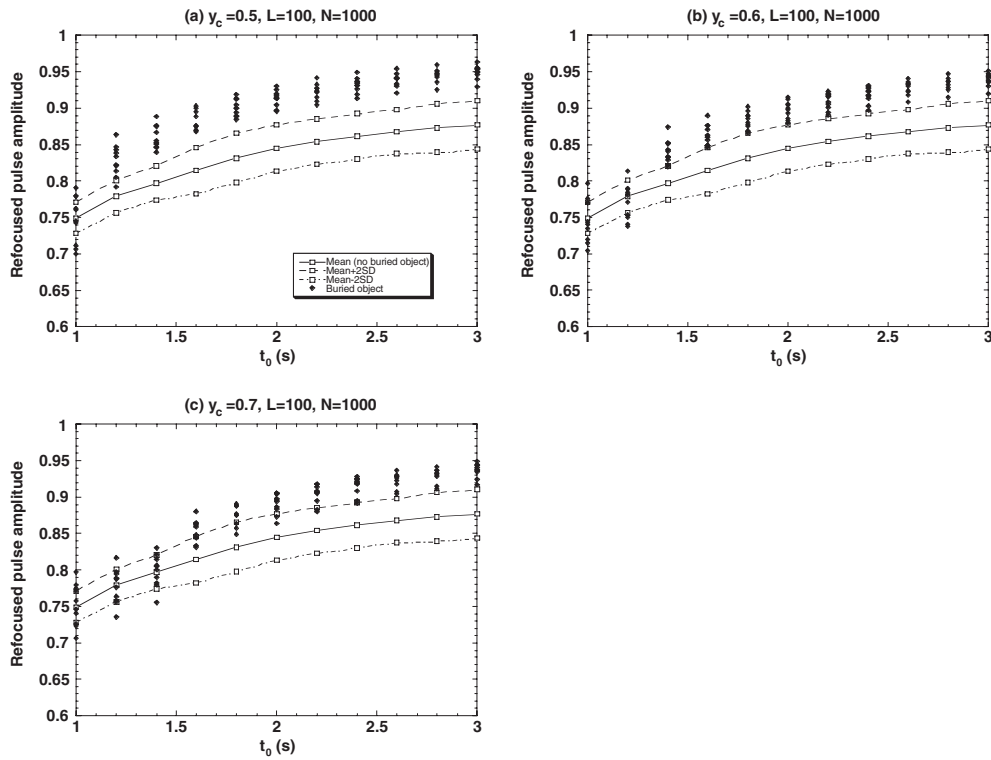


Figure 5. Results of the expanding window time-reversal experiments for ten independent realizations of the medium with buried object of size  $L = 100$  at  $y = y_c$  for three increasing values.

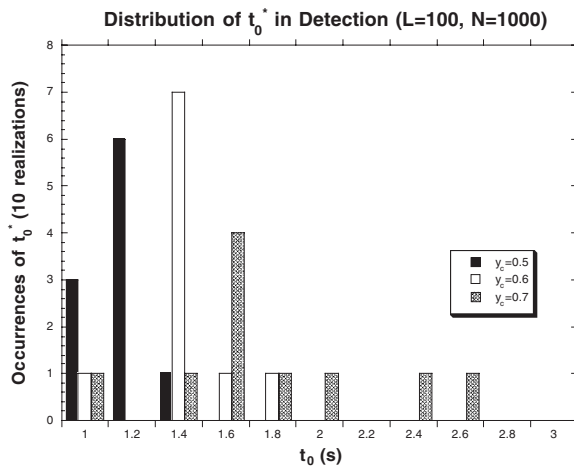


Figure 6. Statistical performance of the detection criterion (20) for ten independent realizations of the medium with buried object of size  $L = 100$  at  $y = y_c$  for three increasing values. The most commonly occurring values of  $t_0^*$  correspond to  $2y_c$  with a systematic bias to the right.

figure 6. For  $y_c = 0.5, 0.6$  and  $0.7$ , the most commonly occurring values of  $t_0^*$ , corresponding to  $2y_c$ , are observed to be 1.2, 1.4 and 1.6, respectively. These critical times correspond to the

first time-reversal recording window that contains reflections from the buried scatterer. Using our criterion (20), detection of scatterer location is most accurate in the case  $y_c = 0.5$ , where all values are within one window increment of the correct value of 1.2. Accuracy reduces as  $y_c$  increases with 8 of 10 cases within one window increment of 1.4 for  $y_c = 0.6$ , and 6 of 10 cases within one window increment of 1.6 for  $y_c = 0.7$ .

In the current study, we considered random media with layers of fixed width  $1/N$ . To assess the potential effects of varying layer widths, we computed refocused pulse amplitudes in the case  $t_0 = 1.0$  s,  $L = 0$  for 50 realizations of the medium. These realizations were obtained by generating a set of random  $c_j$  values (as described earlier) and randomly perturbing the fixed layer widths  $1/N$ . For perturbations of magnitude 0%, 5%, 10% and 15%, statistics (MEAN  $\pm$  SD) of the refocused pulse amplitude were  $0.7523 \pm 0.0248$ ,  $0.7519 \pm 0.0251$ ,  $0.7533 \pm 0.0260$  and  $0.7551 \pm 0.0256$ , respectively. Statistics of the (unsigned) relative error between pulse amplitudes in the fixed and varying layer width cases show a mean close to 1% with a standard deviation of less than 1%. This is in agreement with the theoretical analysis which shows that only the unscaled integrated autocorrelation of the medium  $\int_0^\infty E\{\eta(0)\eta(x)\} dx$  plays a role in the limit  $\epsilon \downarrow 0$ , the correlation length of the medium being of order  $\epsilon^2$  (see [7]).

These results show promise for use of a windowed time-reversal technique in detecting the location of a strong scatterer buried in a randomly layered medium. Inaccuracy in detection of location will likely minimize as the number of layers is increased to enhance self-averaging over the realizations of the random medium. In future studies, we will consider larger scale simulations ( $N \gg 10^3$ ) and note that our frequency domain numerical approach for simulating time reversal is amenable to parallelization.

## 5. Conclusions

Using numerical simulations we have demonstrated that time-reversal refocusing for acoustic pulses shows promise for detection of a strong scatterer buried in a random medium. This is in the regime where the correlation length of the medium is small but where the fluctuations are large, making the detection problem extremely challenging. Our numerical experiments are performed in the acoustic 1D case with a method that is well adapted to more realistic multi-dimensional situations.

## Acknowledgments

The authors would like to thank two referees for their comments and suggestions which improved an earlier version of the paper. This work was supported by grants N00014-02-1-0739 from DARPA and N00014-02-1-0089 from the Office of Naval Research.

## References

- [1] Asch M, Kohler W, Papanicolaou G, Postel M and White B 1991 Frequency content of randomly scattered signals *SIAM Rev.* **33** 519–625
- [2] Asch M, Papanicolaou G, Postel M, Sheng P and White B 1990 Frequency content of randomly scattered signals, Part I *Wave Motion* **12** 429–50
- [3] Bal G and Ryzhik L 2003 Time reversal and refocusing in random media *SIAM J. Appl. Math.* **63** 1475–98
- [4] Beaky M M, Burk J B, Everitt H O, Haider M A and Venakides S 1999 Two dimensional photonic crystal Fabry–Perot resonators with lossy dielectrics *IEEE Trans. Microw. Theory Tech.* **47** 2085–91
- [5] Blomgren P, Papanicolaou G and Zhao H 2002 Super-resolution in time-reversal acoustics *JASA* **111** 230–48
- [6] Borcea L, Tsogka C, Papanicolaou G and Berryman J 2002 Imaging and time-reversal in random media *Inverse Probl.* **18** 1247–79

- 
- [7] Clouet J F and Fouque J P 1997 A time-reversal method for an acoustical pulse propagating in randomly layered media *Wave Motion* **25** 361–8
  - [8] Fink M 1993 Time-reversal mirrors *J. Phys. D: Appl. Phys.* **26** 1333–50
  - [9] Fink M 1999 Time-reversed acoustics *Sci. Am.* (November) 67–93
  - [10] Fouque J P and Solna K 2003 Time-reversal aperture enhancement *SIAM J. Multiscale Model. Simul.* **1** 239–59
  - [11] Haider M A, Shipman S P and Venakides S 2002 Boundary-integral calculations of two-dimensional electromagnetic scattering in infinite photonic crystal slabs: channel defects and resonances *SIAM J. Appl. Math.* **62** 2129–48
  - [12] Papanicolaou G, Postel M, Sheng P and White B 1990 Frequency content of randomly scattered signals, Part II *Wave Motion* **12** 527–49
  - [13] Rokhlin V 1990 Rapid solution of integral equations of scattering theory in two dimensions *J. Comput. Phys.* **86** 414–39
  - [14] Venakides S, Haider M A and Papanicolaou V 2000 Boundary integral calculations of 2-d electromagnetic scattering by photonic crystal Fabry–Perot structures *SIAM J. Appl. Math.* **60** 1686–706